Li diffusion properties of mixed conducting TiO_2-B nanowires

M. Wilkening* and J. Heine
Institute of Physical Chemistry and Electrochemistry, and Center for Solid State Chemistry and New Materials, Leibniz University Hannover, Callinstr. 3a, D-30167 Hannover, Germany

C. Lyness, A. R. Armstrong, and P. G. Bruce†
EaStChem, School of Chemistry, University of St. Andrews, North Haugh, St. Andrews, Fife KY16 9ST, Scotland, United Kingdom
(Received 18 April 2009; revised manuscript received 22 July 2009; published 27 August 2009)

Li_xTiO_2-B nanowires ($0<x\leq 0.9$) are considered to act as promising anode materials in secondary Li-ion batteries. Li self-diffusion parameters in mixed conducting nanowires of the composition $Li_{0.3}TiO_2$ are directly determined by mixing time (t_m)-dependent two-time ^{7}Li spin-alignment echo (SAE) nuclear-magnetic-resonance (NMR) correlation spectroscopy between 330 and 500 K. SAE NMR reveals extremely slow Li self-diffusion processes in Li_xTiO_2-B. Li jump rates τ^{-1} range from 5 to 2.5×10^3 s^{-1}. The corresponding hopping correlation functions F_2 can be well parametrized with stretched exponentials, $F_2 \propto \exp[-(t/t_m)^{\gamma}]$, with an exponent $\gamma=0.35(2)$ being independent of temperature. The influence of spin-diffusion effects on the echo amplitude is elaborated by evolution time-dependent ^{7}Li SAE-NMR experiments. The results are compared with those obtained by conventional ^{7}Li NMR spin-lattice relaxation measurements.

DOI: 10.1103/PhysRevB.80.064302 PACS number(s): 66.30.−h, 76.60.Lz, 82.47.Aa

I. INTRODUCTION

The challenge of reducing global warming and the ever-greater demand for alternative clean energy sources replacing fossil fuels has driven the interest in battery research to an unprecedented level.[1–3] Currently, there is intense interest in materials science to advance fundamental developments in ionically conducting solids for efficient energy storage systems. Electricity generated by wind, wave, or solar power requires sustainable and low-cost energy storage as do hybrid electric vehicles. Research activities are focus on lithium-ion batteries[3–6] which have a higher energy density and lower toxicity than conventional batteries based on lead or nickel. As well as the discovery of new materials, developing efficient batteries requires new techniques to quantify ionic transport. In particular, the latter is crucial when mixed conducting materials have to be studied, i.e., solids which show both electronic and ionic conduction.

Recently, Armstrong *et al.*[7–9] have shown that Li-containing nanowires of TiO_2-B, the fifth polymorph of titanium dioxide, perform well as an anode in secondary (rechargeable) Li-ion batteries. Here, Li_xTiO_2-B represents both an anode material, gaining considerable current interest for applications, and a model substance with which to study mixed conduction with the help of the newly established ^{7}Li spin-alignment echo (SAE) nuclear-magnetic-resonance (NMR) method. SAE NMR is a promising method to characterize macroscopic Li transport from an atomic-scale point of view.[10–13] Generally, conventional NMR methods are well suited to quantify lithium diffusion parameters on a long length scale, as recently outlined by us using different model substance such as polycrystalline Li_xTiS_2 as well as glassy $LiAlSi_2O_6$, see Refs. 14–16. However, in the case of mixed conductors the capabilities of standard NMR techniques to probe dynamic properties are significantly limited because of the rather short NMR relaxation rates in these materials which result from the coupling of Li spins with conduction electrons and/or interactions of Li^+ with paramagnetic centers. Note the presence of mixed Ti^{3+}/Ti^{4+} valence states in Li_xTiO_2-B. Therefore, NMR spin-lattice relaxation rates (in the laboratory as well as rotating frame of reference) are expected to show only shallow temperature dependencies since they are not dominated by diffusion-induced contributions. Consequently, the extraction of reliable diffusion parameters such as Li jump rates or activation energies from NMR spin-lattice relaxation data is fraught with difficulties and far from straightforward.

The present paper greatly extends a short letter version[17] and includes preparation time-dependent NMR measurements which are crucial for a detailed analysis of the features of spin-alignment echoes. We will show how the measurement of mixing and preparation time-dependent ^{7}Li NMR spin-alignment echoes can be used to study the diffusion properties of Li_xTiO_2-B nanowires with the nominal composition $x=0.3$. Taking into account background effects such as temperature-independent spin diffusion we were able to record purely diffusion-induced echo decay curves from which the diffusion parameters can be directly obtained. Interestingly, Li^+ self diffusion in Li_xTiO_2-B turned out to be rather slow.[17] Nonetheless, facile incorporation and removal of Li is possible when the nanowires are used as an anode in a lithium-ion battery. This suggests that the shorter diffusion length in nanostructured materials compensates for the observed slow Li self diffusivity probed by ^{7}Li SAE NMR.

II. SPIN-ALIGNMENT ECHO NMR

The ^{7}Li spin-alignment echo NMR technique, which is described in detail in Ref. 18, probes slow Li self-diffusion processes by taking advantage of the interaction of the nuclear quadrupole moment of the ^{7}Li spin (spin quantum number $I=3/2$) with a nonvanishing electric field gradient (EFG) tensor at the site of the nucleus. The respective secular part of the first-order quadrupolar interaction is given by

the following Hamiltonian $\hat{H}_Q$ which can be expressed by the product of the irreducible spherical tensor operator $\hat{T}_{lm}$ of rank $l=2$ and order $m=0$, and the quadrupole precession frequency ω_Q,

$$\hat{H}_Q = \frac{\sqrt{6}}{2I(2I-1)}\omega_Q \hat{T}_{20} \tag{1}$$

with ω_Q and $\hat{T}_{20}$ given by

$$\omega_Q = \frac{1}{4}\frac{e^2qQ}{\hbar}[3\cos^2\theta_Q - 1 - \eta_Q \sin^2\theta_Q \cos(2\phi_Q)] \tag{2}$$

and

$$\hat{T}_{20} = \frac{1}{\sqrt{6}}[3\hat{I}_z^2 - \hat{I}(\hat{I}+1)]. \tag{3}$$

Here, the angles θ_Q and ϕ_Q specify the orientation of the EFG tensor at the Li site with respect to the external magnetic field. $\hat{I}_z$ and $\hat{I}$ represent the nuclear-spin operators. η_Q denotes the asymmetry and $\delta_Q = e^2qQ/(2\hbar)$ the anisotropy parameter. Usually the strength of the quadrupole coupling is discussed in terms of the quadrupole coupling constant $C_Q = e^2qQ/h$, where e and eq are the proton charge and the principle component of the electric field gradient tensor, respectively. Q is the quadrupole moment of the nucleus and h is Planck's constant. C_Q usually is on the order of a few tens of kHz. Second-order quadrupolar shift interactions are negligible when using an external magnetic field strength B_0 of the order of several tesla.

The principle of SAE NMR is the following. Different crystallographic Li sites are characterized by a specific EFG and thus by a specific quadrupole precession frequency ω_Q. Jumping of the ion between electrically inequivalent sites renders ω_Q time dependent and can be used to record single-particle hopping correlation functions S_2 provided the EFGs themselves are independent of time. S_2 yields information about dynamic as well as geometric information about the diffusion process.[18,19] Its analogy to quasielastic neutron scattering, operating on a much shorter time scale, was explicitly treated in Refs. 20 and 21. The pulse sequence used to sample correlation functions was introduced by Jeener and Broekaert (JB).[22] Its systematic application to spin-3/2 nuclei such as ^{7}Li or ^{9}Be was initialized by Tang and Wu[23–25] as well as by Böhmer *et al.*[26] followed by a number of further studies utilizing also the ^{6}Li isotope with its much smaller Q value.[10–16,27–33] The JB sequence reads as follows:

$$\beta_{1_{\phi_1}} - t_p - \beta_{2_{\phi_2}} - t_m - \beta_{3_{\phi_3}} - t_p - \text{echo}.$$

β_i denote the pulse lengths and ϕ_i the respective phases. Note that proper phase cycling is needed to suppress unwanted coherences.[19] The preparation time is denoted as t_p and the mixing period as t_m. Starting from $\hat{I}_z$, the first two pulses, separated by a short t_p in the case of ^{7}Li, generate a spin-alignment state according to

$$\hat{T}_{10} \xrightarrow{\beta_1\hat{I}_{\phi 1},\hat{H}_Q t_p,\beta_2\hat{I}_{\phi 2}} -\frac{1}{2}\sqrt{\frac{3}{2}}\sin\beta_1 \sin(2\beta_2)\sin(\omega_Q t_p)\hat{T}_{20} \tag{4}$$

if ϕ_1 and ϕ_2 differ by 90°. The third pulse transforms quadrupolar alignment back into a detectable transverse magnetization via

$$-\frac{1}{2}\sqrt{\frac{3}{2}}\sin\beta_1 \sin(2\beta_2)\sin(\omega_Q t_p)\hat{T}_{20} \xrightarrow{\beta_3\hat{I}_{\phi 3},\hat{H}_Q t(=t_p)} \times\frac{9}{20}\sin\beta_1 \sin(2\beta_2)\sin(2\beta_3) \times\sin[\omega_Q(t_m=0)t_p]\sin[\omega_Q(t_m)t_p]. \tag{5}$$

The amplitude of the sin-sin stimulated echo generated after the third (reading) pulse can be maximized when the pulse lengths are chosen to be $\beta_1=\pi/2$ and $\beta_2=\beta_3=\pi/4$, respectively. For a powder average, denoted by the angular brackets $\langle\ldots\rangle$, the echo amplitude reads

$$S_2'(t_p,t_m,t) = \frac{9}{20}\langle\sin[\omega_Q(t_m=0)t_p]\sin[\omega_Q(t_m)t_p]\rangle. \tag{6}$$

Generally, t_p is chosen to be smaller than the transverse relaxation time T_2 and is kept constant. t_m varies from about 10 μs up to the second range. The damping of $S_2 \propto \exp[-(t_m/\tau_{\text{SAE}})^\gamma]$ with $0<\gamma\leq 1$ is either due to (i) successful hops of the ions implying $\sin[\omega_Q(t_m=0)t_p] \neq \sin[\omega_Q(t_m)t_p]$ and/or (ii) due to other effects such as quadrupolar spin-lattice relaxation (characterized by the time constant T_{1Q}) or spin diffusion ($T_{1\text{SD}}$) leading to an additional echo damping according to

$$S_2 \propto \exp[-(t_m/\tau_{\text{SAE}})^\gamma]\exp[-(t_m/T_{1Q})^{\gamma'}]\exp[-(t_m/\tau_{1\text{SD}})^{\gamma''}] \approx \exp[-(t_m/\tau_\varepsilon)^{\gamma_\varepsilon}]. \tag{7}$$

Combining the two latter terms to a new one representing nondiffusive echo damping in general, and disregarding the constant prefactor of Eq. (6), i.e., focusing on normalized echo amplitudes ranging between 0 and 1, the diffusion-induced contribution of S_2' is represented by

$$F_2 \equiv S_2/\{\exp[-(t_m/\tau_{\text{ND}})^{\gamma_{\text{ND}}}]\} = \exp[-(t_m/\tau_{\text{SAE}})^\gamma]. \tag{8}$$

The damping factor $S_{\text{ND}}=\exp[-(t_m/\tau_{\text{ND}})^{\gamma_{\text{ND}}}]$ with $0<\gamma_{\text{ND}}\leq 1$ determines the lower limit of detectable decay rates, i.e., only if $\tau_{\text{SAE}}<\tau_{\text{ND}}$ holds, NMR experiments are reasonable. Note, $\tau_{1\text{SD}}$ is usually on the order of seconds whereas T_{1Q} is theoretically given by the relation $T_1/T_{1Q}=25/8$, where T_1 is the spin-lattice relaxation time.[33] However, deviations from this ratio have been already observed.[33] Since the ratio $\tau_{\text{SAE}}/\tau_{\text{ND}}$ varies with temperature over several orders of magnitude (see below) it is possible to discriminate between F_2 and nondiffusive background effects.[13] Usually a weak temperature dependence is expected for τ_{ND} at very low temperatures, i.e., in the range $\omega_0\tau \gg 1$ where the motional correlation time of the Li spins is negligible compared to ω_0, see Ref. 15. In this T range the S_2 decay is solely determined by $\exp[-(t_m/\tau_{\text{ND}})^{\gamma_{\text{ND}}}]$ so that F_2, being exclusively influenced by Li^+ hopping, will be available from the S_2 data recorded at intermediate T. At even higher temperatures solely the F_2-decay curve is measured or can be easily separated from

background effects, e.g., when S_2 exhibits a two-step behavior. This is generally expected for crystalline materials if the difference between τ_{SAE} and τ_{ND} is large enough (see below).

III. EXPERIMENT

TiO_2-B nanowires were prepared from NaOH and TiO_2 (anatase) following a hydrothermal synthesis route. Details of the sample preparation as well as the electrochemical insertion of Li are described elsewhere, see Refs. 7 and 8 including also the characterization of the sample.

^{7}Li-stimulated echoes were mainly recorded on a Bruker MSL 400 spectrometer connected to a shimmed Oxford cryomagnet with a nominal field of 9.4 T. An MSL 100 console in combination with a field-variable magnet was used to perform some measurements at 77.72 MHz. We have used commercial broadband probes (Bruker) designed to operate well between 123 and 433 K. For instance, the $\pi/2$ pulse length was about 4.5 μs at a resonance frequency of 155.45 MHz. The temperature was monitored via an Oxford temperature controller (ITC) in combination with a NiCr-Ni thermocouple placed near the sample which was sealed in a quartz tube under vacuum. The three-pulse sequence of Jeener and Broekaert[22] was employed to record the echoes. Spin-lattice relaxation rates in both the laboratory and rotating frame of reference ($1/T_1$ and $1/T_{1\rho}$) were recorded using standard pulses sequences[34] such as the well-known recovery saturation experiment and the spin-lock technique. For the latter measurements we used a locking frequency of 14(2) kHz. See Ref. 15 for details of the NMR setup.

IV. RESULTS AND DISCUSSION

Usually ^{7}Li NMR spin-alignment two-time correlation functions are recorded for variable mixing times t_m and a very short preparation time t_p being typically less than 20 μs. The shorter t_p is the better unwanted *dipolar* contributions of the stimulated echo can be suppressed. Such contributions arise from homonuclear ^{7}Li-^{7}Li interactions leading to "central resonances" in the corresponding SAE-NMR spectrum obtained after Fourier transformation of the echoes. Such effects are explicitly treated in Refs. 30 and 35, for example. In the ideal case, which is, e.g., present when electric-quadrupole interactions are much larger than the magnetic dipolar ones, the spin-alignment spectra of a spin-3/2 nucleus such as ^{7}Li are composed of satellite intensities only.[12,18]

In order to determine up to which preparation times t_p-stimulated echo NMR measurements are reasonable in the present case and how the evolution of *quadrupolar* and *dipolar* echo intensities scale with t_p, we will focus briefly on a range of echoes recorded at various preparation times t_p (5–300 μs) and fixed mixing times t_m. Typical ^{7}Li NMR stimulated echoes of $Li_{0.3}TiO_2$ nanowires are shown in Fig. 1(a). A very short mixing time of 10 μs ensures that the decay of S is not influenced by Li^+ hopping taking place at the temperature chosen (343 K) for this echo analysis. Even at very short preparation times t_p of less than 10 μs the stimulated echoes are composed of two parts: besides the sharp decaying quadrupole part a second echo presumably arising from homonuclear dipole-dipole interactions is evident.[30] The echoes recorded at different t_p values can be roughly fitted with a combination of two Gaussian functions according to

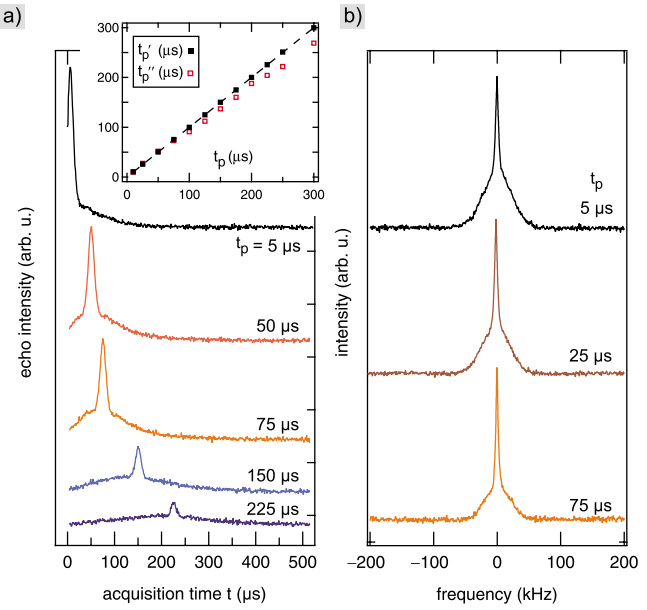

FIG. 1. (Color online) (a) ^{7}Li NMR stimulated echoes of polycrystalline $Li_{0.3}TiO_2$ nanowires recorded at various preparation times t_p and for t_m=10 μs. (T=343 K, $\omega_0/2\pi$=155.45 MHz). The echoes are composed of a sharp decaying quadrupole and a slowly decaying dipolar part. At t_p=5 μs the ratio of the corresponding amplitudes s_q/s_d is about six. Inset: position of the quadrupolar (t_p') and dipolar (t_p'') echoes vs t_p [cf. Eq. (9)]. The dashed line refers to $t_p'=t_p''=t_p$. (b) ^{7}Li NMR stimulated-echo spectra obtained from the echoes shown on the left side. They were obtained after Fourier transformation of the echoes beginning from the top of the quadrupolar contribution, i.e., at $t=t_p$.

$$S(t_p,t_m\to 0,t) = s_q(t_p)\exp\{-[(t-t_p')^2\sigma_q^2/2]\} + s_d(t_p)\exp\{-[(t-t_p'')^2\sigma_d^2/2]\}, \quad (9)$$

where t_p' and t_p'' specify the shift of the respective echo maximum with respect to the expected position at $t=t_p$. Here, after taking into account receiver dead-time effects of about 2 μs, the maximum of the quadrupolar echo shows up exactly at $t=t_p$, i.e., $t_p'=0$. Within an accuracy of less than $\pm 5\%$ this holds also for the dipolar contribution if $t_p<100$ μs. For larger t_p we observed a slight shift obeying the relation $t_p''=0.91(1)t_p$. In the range $5\le t_p\le 100$ μs the ratio of the variances σ_q and σ_d of Eq. (9), representing electric quadrupolar and magnetic dipolar interactions, respectively, is given by $\sigma_q/\sigma_d\approx 10$. As an example, at t_p=25 μs we obtain $\sigma_q = 0.156(2)\times 10^6$ rad s^{-1} and $\sigma_d=0.0154(3)\times 10^6$ rad s^{-1}. The corresponding shifts are $t_p'=25.7(1.2)$ μs and $t_p'' = 27.4(2.2)$ μs, respectively. Whereas σ_q seems to be independent of preparation time, σ_d depends on t_p if the preparation time is chosen to be larger than 100 μs. For example, at t_p=300 μs it decreased to $0.0087(3)\times 10^6$ rad s^{-1}. This trend is also observed at much lower temperatures of about

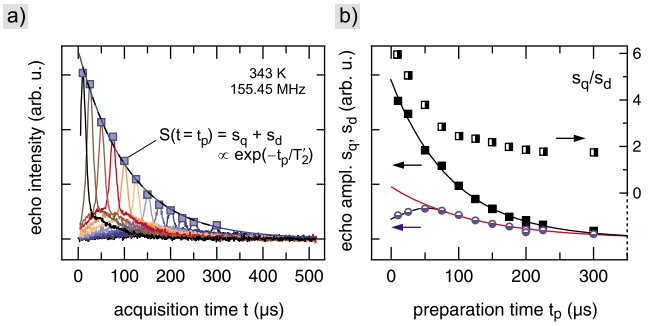

FIG. 2. (Color online) (a) Decay of the total ^{7}Li NMR echo amplitude $S(t_p, t_m \to 0, t = t_p) = s_q(t_p) + s_d(t_p)$ as a function of preparation time. (b) Left axis: $s_q(t_p)$ and $s_d(t_p)$ vs t_p. Right axis: the ratio $s_q(t_p)/s_d(t_p)$ vs t_p. Data were recorded at $T = 343$ K and a resonance frequency of 155.45 MHz

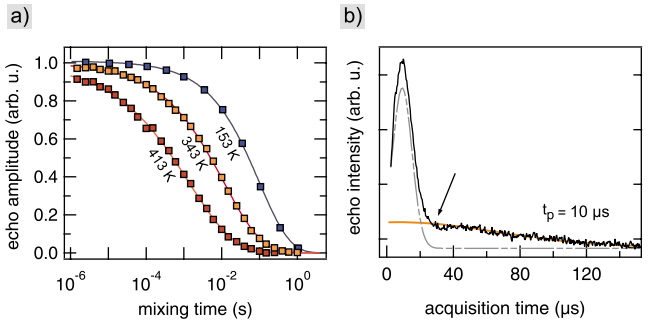

FIG. 3. (Color online) (a) ^{7}Li SAE-NMR two-time correlation functions of $Li_{0.3}TiO_2$ nanowires recorded at $T = 153$, 343, and 413 K. The decay curves were recorded at $t_p = 10$ μs and 155.45 MHz. (b) ^{7}Li SAE-NMR echo recorded at $t_m = 100$ μs and $t_p = 10$ μs, respectively, showing its decomposition into the quadrupolar (dashed line) and dipolar echo (solid line). The arrows marks a small undershoot of the signal appearing when $t_p \approx 10$ μ is chosen. This feature gives rise to slightly distorted spin-alignment spectra, see Ref. 27 for analogous results obtained for polycrystalline Li_4SiO_4.

180 K. It is worth noting that σ_d of an SAE-NMR experiment should not be mixed with the corresponding value of a solid-echo NMR experiment.[29]

Fourier transformation of the echoes beginning from their tops leads to the two-component NMR-stimulated echo spectra displayed in Fig. 1(b). The broad contribution refers to the sharp decaying component whereas the superimposed narrow one reflects the slowly decaying dipolar part of the corresponding echo. The linewidth (full width at half maximum) of the Gaussian-shaped quadrupole contribution is, when, e.g., an echo recorded at $t_p = 25$ μs is analyzed, about $\Delta_q = 56.8$ (1.0) kHz reflecting a rather large distribution of different EFGs the Li ions are exposed to in nanowires of $Li_{0.3}TiO_2$. According to the relation $\Delta_q = (\sigma_q \sqrt{8 \ln 2})/(2\pi)$, which is valid for a Gaussian distribution of frequencies, this yields $\sigma_q = 0.152(3) \times 10^6$ rad s^{-1}. Practically the same value is obtained from the time-domain data (see above). Δ_d is about 5.8(2) kHz leading to $\sigma_d = 0.0155(5) \times 10^6$ rad s^{-1}.

As can be seen in Fig. 1(a), the amplitudes s_q and s_d, which refer to the two parts of the echoes recorded at $T = 343$ K, do not show the same t_p dependence. Whereas the quadrupole echo is already fully developed at about $t_p = 5$ μs, the broader dipolar one reaches its maximum at a longer preparation time of $t_p = 50$ μs. This behavior reflects approximately the ratio of the strengths of the two interactions (see above). At $t_p \to 0$ the ratio s_q/s_d is about 6, whereas at $t_p = 50$ μs the amplitude $s_q(t_p)$ is already decreased to about 60% of its initial value $s_q(0)$ [see Fig. 2(b)]. The decay of $s_q(t_p)$, and above $t_p = 50$ μs also that of $s_d(t_p)$, follows a single exponential. Whereas the total echo amplitude S is proportional to $\exp(-t_p/T'_2)$ with $T'_2 = 108(4)$ μs the characteristic transversal decay times of $s_q(t_p)$ and $s_d(t_p)$ are 91(3) and 122(4) μs, respectively. At a sufficiently long preparation time t_p, the ratio $s_q(t_p)/s_d(t_p)$ reaches a value of about 2. This is in agreement with calculated ratio of 2.02 reported by Tang and Wu, see Ref. 24 for an metallic glass for which chemical *and* Knight-shift interactions are not negligible. Thus, besides homonuclear dipole-dipole interactions, coupling to conduction electrons and/or unlike dipolar interactions between the ^{7}Li spins and paramagnetic centers have to be taken into account, too, when explaining the origin of the unwanted dipolar contribution of the spin-alignment echo NMR spectra.

The echo analysis shows that, as expected for a quadrupole nucleus such as ^{7}Li, suppression of dipolar echo intensities works well when t_p is chosen as short as possible.[24] Since a clear determination of s_q and s_d is also possible for larger t_p with values up to 100 μs, we have in addition carried out mixing time-dependent ^{7}Li SAE-NMR measurements at longer preparation times than 10 μs. In general, the sensitivity of SAE NMR with respect to temporal changes in ω_Q increases the larger t_p is set.

Three selected two-time correlation functions $S_2(t_p, t_m, t)$ of $Li_{0.3}TiO_2$, which were recorded at fixed $t_p = 10$ μs, are plotted as a function of mixing time t_m in Fig. 3(a). The echo amplitude S_2, which was determined at $t = t_p$, takes only the intensities of the quadrupole echoes into account. Prior to the determination of S_2 the Gaussian-shaped dipolar contribution [cf. Fig. 3(b)] was subtracted from the total echo $S(t_p, t_m, t)$ for each mixing time (10 $\mu s \le t_m \le 1$ s) leading to $S_2(t_p, t_m) = s_q(t_p, t_m)$. The temperature-dependent decay curves $S_2(t_p, t_m)$ can be well parametrized with stretched exponentials $S_2(t_p, t_m) \propto \exp\{-[t_m/\tau_\varepsilon(t_p)]^\gamma_\varepsilon\}$ reflecting the superposition of different damping factors [see Eq. (7)]. The corresponding decay rates $1/\tau_\varepsilon$ are plotted in Fig. 4 vs the inverse temperature. At temperatures $T < 220$ K we found $1/\tau' \approx 1/\tau_{ND}(t_p)$ as deduced from the very weak temperature dependence of the decay rate in this low-T range. Note that τ^{-1}_{ND} depends significantly on t_p, see below. The normalized S_2 curve recorded at the lowest accessible temperature of 153 K (Fig. 4) is given by $S_{2,153\ K}(t_p) = S_{ND}(t_p) = \exp\{-[t_m/114(5)\ \text{ms}]^{0.60(5)}\}$. According to Eq. (8) it is used to obtain the $F_2(t_p, t_m)$ curves and therefore to determine $1/\tau_{SAE}$. At intermediate T the decay curves are given by Eq. (7), whereas in the limit of high temperatures ($T > 400$ K) they are solely damped by Li jump processes, i.e., $S_{2,413\ K} \approx F_{2,413\ K}$. The F_2 curves [cf. Fig. 5(a)] are characterized by the same, temperature-independent stretching exponent $\gamma = 0.35(2)$ [see Fig. 6(a)] indicating that between 300 and 450 K the same Li diffusion process is probed. In Fig. 6(a) the temperature dependence of γ_ε as well as that of the γ values

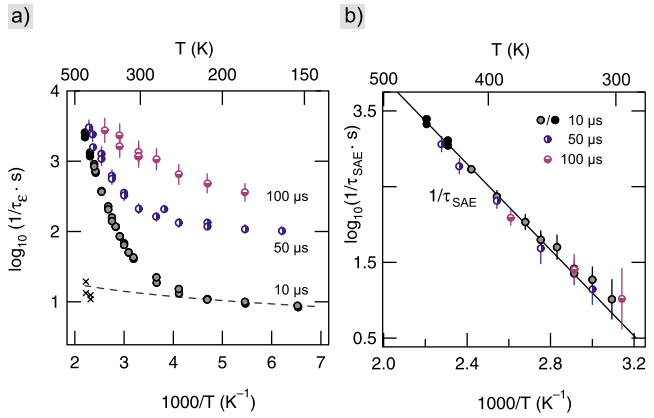

FIG. 4. (Color online) (a) Decay rates $\tau_\varepsilon^{-1}=f(t_p)$ obtained from the $S_2(t_p,t_m)$ (see Fig. 3) as a function of the inverse temperature. The rates were recorded at the preparation times indicated. $\tau_\varepsilon^{-1}(T)$ can be subdivided into three regions: below $T=220$ K the rate τ_ε^{-1} approximates τ_{ND}^{-1}; at intermediate temperatures it is governed by Eq. (7) whereas at higher T the decay rate is given by $\tau_\varepsilon^{-1}\approx\tau_{SAE}^{-1}$. Above 335 K $\tau_{SAE}^{-1}(\bullet)$ can be directly obtained from S_2 because of its two-step decay behavior [Eq. (11)]. The dashed line indicates the sublinear temperature dependence of τ_{ND}^{-1} following a power law $\tau_{ND}^{-1}\propto T^{0.6(1)}$. Crosses ($\times$) display the rates $\tau_{ND}^{\prime-1}$ as deduced from the two-step S_2-decay curves recorded around $T=453$ K. (b) Temperature dependence of the τ_{SAE}^{-1} rates determined according to Eq. (8). τ_{SAE}^{-1} is independent of t_p indicating Li jumps between sites characterized by quite different EFGs.

obtained from the F_2 curves are shown. For better comparison, in Fig. 5(a) $F_{2,343\ K}$ and $S_{2,343\ K}$ are shown as examples. The decay rates $1/\tau_{SAE}(1/T)$ [see Eq. (8)] recorded at $t_p=10$ μs are presented in Fig. 4(b). They follow an Arrhenius relation according to

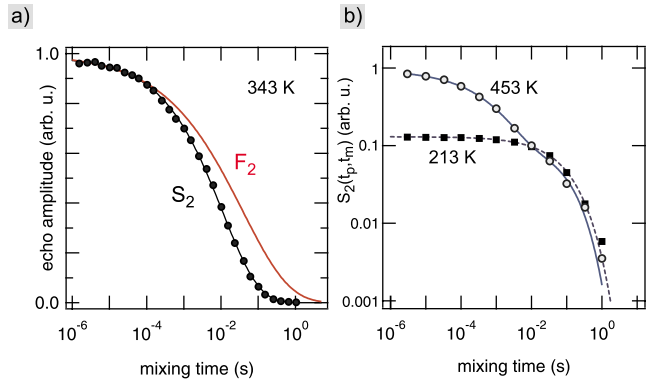

FIG. 5. (Color online) (a) Comparison of $S_2(t_p=10\ \mu s,t_m)$ and $F_2=S_2/S_{ND}=S_2/\{\exp[-(t_m/\tau_{ND})^{\gamma_{ND}}]\}$ with $\tau_{ND}=114(5)$ μs and $\gamma_{ND}=0.60(5)$, respectively. S_2 was recorded at 343 K and 155.45 MHz. (b) ^{7}Li NMR two-time correlation function S_2 which was recorded at $T=453$ K. It shows a two-step decay behavior. The solid line shows a fit according to Eq. (11). The second decay step showing up at larger t_m reflects S_{ND} which is shown for comparison, too. Note that S_{ND} depends strongly on t_p [see Fig. 6(b)] and only weakly on temperature. For comparison, S_{ND}, which is scaled such that its maximum is given by S_∞, is also shown.

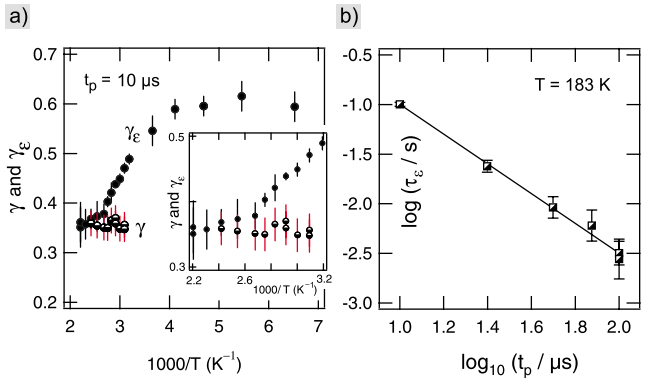

FIG. 6. (Color online) (a) Temperature dependence of γ_ε obtained from the S_2 decay curves recorded at $t_p=\mu$s. At low temperatures γ_ε approaches $\gamma_{ND}\approx 0.6$ whereas at the highest T we found $\gamma_\varepsilon\approx\gamma$. Inset: magnification of the data ranging from 313 to 450 K. (b) $\tau_\varepsilon(t_p)$ recorded between $t_p=10$ and 100 μs, and measured at $T=183$ K and 155.45 MHz. The solid line shows a fit according to $\tau_\varepsilon(t_p)\propto t_p^{1.5(1)}$.

$$\tau_{SAE}^{-1}=\tau_{0,SAE}^{-1}\exp[-E_a/(k_BT)], \tag{10}$$

where k_B is Boltzmann's constant. The activation energy E_a and the pre-exponential factor $\tau_{0,SAE}$ are 0.56(3) eV and $2.5(5)\times10^{-10}$ s^{-1}, respectively. The fit shown in Fig. 4(b) considers the rates recorded at $t_p=10$ μs and takes into account the individual errors of the data points which increase with decreasing T, i.e., when S_2 approaches S_{ND}. Interestingly, when τ_ε becomes less than 1 ms and the ratio $\tau_{ND}/\tau_\varepsilon$ reaches approximately 100, which is fulfilled at temperatures higher than 430 K and a very short preparation time of 10 μs, the S_2 decay curves exhibit a two-step behavior according to

$$S_2(t_p,t_m)=\{[1-S_\infty(t_p)]F_2+S_\infty(t_p)\}\exp[-(t_m/\tau'_{ND})^{\gamma_{ND}}] \tag{11}$$

with $F_2(t_p,t_m)=\exp[-(t_m/\tau_{SAE})^\gamma]$. As an example, in Fig. 5(b) $S_{2,453\ K}(t_p,t_m)$ vs t_m is shown in a double-logarithmic plot. The plateau value turned out to be about 0.13(3). For comparison, $S_\infty\cdot S_{ND}$ is also included in the figure. Generally, S_∞ is related to the number N of electrically inequivalent Li sites the ions visit along their diffusion pathway via $S_\infty=1/N$.[19] However, as shown recently S_∞ can be additionally affected by influences of homonuclear dipole-dipole couplings leading to smaller values than expected crystallographically.[30] For comparison, the rates $\tau_{ND}^{\prime-1}$ are also included in Fig. 4(a). As expected, they are in good agreement with the rates $\tau_{ND}(T)$ after extrapolation these to higher T according to $\tau_{ND}(T)\propto T^{0.6(1)}$ (see dashed line in Fig. 4).

As shown in Fig. 4(a) as well as temperature, τ_{ND} depends also on the preparation time t_p chosen. This is explicitly shown for $T=183$ K in Fig. 6(b). The solid line corresponds to $\tau_{ND}(t_p)\propto t_p^{1.5(1)}$. A t_p^2 dependence would point to an echo damping which is caused by small frequency changes the ions are exposed to—a situation which is comparable to that of spin diffusion. The deviation found here indicates that the S_{ND} decay is presumably affected by additional processes

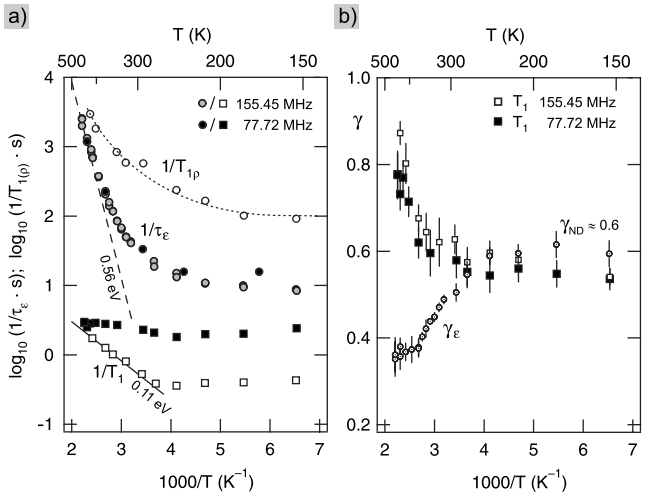

FIG. 7. (a) Arrhenius plot of τ_{ε}^{-1} recorded at two different radio frequencies viz 155.45 and 77.72 MHz. For comparison, the corresponding spin-lattice relaxation rates measured in the laboratory (T_1^{-1}) and rotating frame of reference ($T_{1\rho}^{-1}$) are also shown. The dotted line is to guide the eye. The dashed one indicates the fit of the $\tau_{\mathrm{SAE}}^{-1}(t_p=10\ \mu\mathrm{s})$ rates shown Fig. 4. The solid line represents a fit according to the Arrhenius law $T_1^{-1} \propto \exp[-E_a'/(k_B T)]$. Note the frequency dependence of T_1^{-1} and its absence for τ_{ε}^{-1}. Below 250 K the ratio $T_1(155.45\ \mathrm{MHz})/T_1(77.72\ \mathrm{MHz})$ is about five. See text for further details. (b) Temperature dependence of the stretching factors which were obtained after parametrizing the magnetization transients of the NMR spin-lattice relaxation measurements with stretched exponentials. For comparison, $\gamma_{\varepsilon}(1/T)$ is also shown.

such as coupling of the spins with paramagnetic centers. However, although a relatively strong dependence of τ_{ε} is observed at low T, the corresponding F_2 curves determined at $t_p=50\ \mu\mathrm{s}$ and $t_p=100\ \mu\mathrm{s}$, respectively, are much less affected by this circumstance. The above mentioned correction procedure yields τ_{SAE}^{-1} rates which are independent of t_p [see Fig. 4(b)] indicating that the ^{7}Li SAE-NMR measurements performed are sensitive to Li^+ jumps between sites characterized by quite different EFGs.

Additionally, we have carried out SAE-NMR experiments using a smaller magnetic field strength B_0 corresponding to a ^{7}Li resonance frequency of $\omega_0/2\pi=77.72$ MHz (Fig. 7). Above 250 K the corresponding $S_2(t_p=10\ \mu\mathrm{s}, t_m)$ decay curves coincide with those measured at larger magnetic field. Whereas the rates τ_{ε}^{-1} turn out to be independent of ω_0, which is expected for a motional correlation rate, the corresponding spin-lattice relaxation rates T_1^{-1} measured at 77.72 and 155.45 MHz, respectively, clearly exhibit a frequency dependence. For example, decreasing the external magnetic field B_0 by a factor of 2 leads to an increase in $T_1^{-1}(100\ \mathrm{K})$ from about 1 s^{-1} to approximately 3.2 s^{-1} while the corresponding rates τ_{ε}^{-1} are 217(5) s^{-1} and 208(7) s^{-1}, respectively. The magnetization transients from which the T_1^{-1} rates were extracted can be parametrized by stretched exponentials only. The respective stretching factors are shown in Fig. 7(b) as a function of inverse temperature. For comparison, those of the ^{7}Li SAE-NMR measurements are also included.

Below 250 K the rates $T_1^{-1}(1/T)$ measured at 155.45 MHz are governed by nondiffusive background effects. Above room-temperature longitudinal relaxation is primarily induced by short-range Li diffusion. The solid line in Fig. 7 yields $E_a'=0.11$ eV. It represents the low-T flank of the rate peak $T_1^{-1}(1/T)$ whose maximum is expected when the motional correlation time τ reaches the order of the inverse Larmor frequency $\omega_0=2\pi\times 155.45$ MHz, i.e., when τ is about 1 ns.

Reducing the resonance frequency to 77.72 MHz leads to a strong increase in T_1^{-1} so that the relevant diffusion-induced contributions of T_1^{-1} cannot be separated out any more. Similar to τ_{ND}^{-1}, the short and almost temperature-independent background rate showing up below 250 K is presumably caused by coupling of the spins with conduction electrons and the interaction with paramagnetic centers in $Li_{0.3}TiO_2$. Note, the stretching factors of both the T_1 magnetization transients at 77.72 MHz as well as those recorded at 155.45 MHz approximate a value of about 0.55 which is similar to γ_{ND} of SAE NMR [see Fig. 7(b)]. This observation reinforces the assumption that the mechanism-inducing ^{7}Li NMR spin-lattice relaxation appears likely to be identical to that causing the damping of the corresponding stimulated echoes.

Expectedly, measurements of spin-lattice relaxation rates $T_{1\rho}^{-1}$ in the rotating frame of reference, which were carried out using a locking frequency of approximately 14 kHz, are fraught with the same difficulties inhering the T_1^{-1} measurements at 77.72 MHz. Therefore, below $T=450$ K a pronounced diffusion-induced flank and thus a reliable activation energy cannot be extracted from such data in the present case. As indicated in Fig. 7(a), we expect that the rates $T_{1\rho}^{-1}(1/T)$ follow an Arrhenius law with the same activation energy as probed by SAE NMR before the diffusion-induced rate maximum is reached.

The discrepancy between the activation energies probed by spin-lattice relaxation (0.11 eV) on the one hand and SAE NMR (0.56 eV) on the other hand might be explained by the different time and length scales to which the two methods are sensitive. In the case of SAE NMR long-range transport parameters are probed[10] while in the limit $\tau\omega_0 \gg 1$ the rate T_1^{-1} is mainly controlled by (localized) short-range Li dynamics. Taken together, this points to a highly heterogeneous nature of Li hopping in $Li_{0.3}TiO_2$-B which becomes also apparent regarding the strongly stretched F_2 correlation functions pointing to a broad distribution of jump rates. This is corroborated by ^{7}Li NMR line-shape measurements. In Fig. 8(a) the linewidth (full width at half maximum) of the NMR central transition of $Li_{0.3}TiO_2$-B nanowires is plotted against temperature. As can be clearly seen, motionally induced narrowing of the ^{7}Li NMR line [Fig. 8(b)], which is due to averaging of ^{7}Li dipolar interactions with increasing τ^{-1}, extends over quite a large temperature range of nearly 300 K. This reflects the presence of a large distribution of hopping processes taking place on different length scales.

When interpreting activation energies deduced from spin-lattice relaxation NMR measurements one should keep in mind that the slope of the low-T flank can also be affected by correlation effects resulting from Coulomb interactions between the moving ions and/or structural disorder. Such a situation usually leads to much smaller slopes and thus activation energies than expected. Therefore, the interpretation

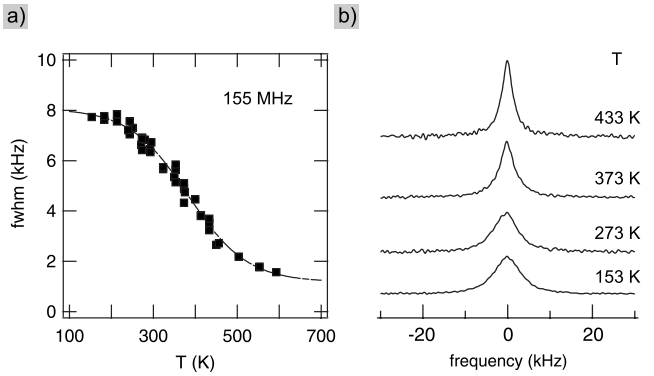

FIG. 8. (a) ^{7}Li NMR linewidths (full width at half maximum) of Li intercalated TiO_2-B nanowires vs temperature. The solid line is to guide the eye. (b) Corresponding ^{7}Li NMR spectra recorded at 155.45 MHz and at the temperatures T indicated.

of activation energies deduced from NMR relaxation measurements is less straightforward compared to that of SAE NMR. In particular, this is the case when the observed NMR spin-lattice relaxation behavior deviates from standard theory introduced by Bloembergen *et al.*[36] predicting $T_1^{-1} \propto \omega_0^{-2}$ in the limit $\tau\omega_0 \gg 1$. If on the other hand correlation effects are mostly absent and a solitary diffusion mechanism prevails, the differences are expected to be much smaller or even vanish when an elementary jump process can be identified as the relevant transport mechanism.[15] In such a case the shape of the hopping correlation function is mainly determined by the dimensionality of the diffusion process and might deviate from a pure exponential. Note that in the present case Li diffusion is anticipated to be primarily confined to two dimensions in the TiO_2-B structure. The presence of a low-dimensional diffusion process might additionally influence the stretching exponent γ.

Whereas the stretching factors of Fig. 7(b) of the T_1 and SAE-NMR measurements behave quite similar at low temperatures as discussed above, they show the opposite temperature dependence for $T > 300$ K. While γ_ε decreases with increasing T reaching the final value $\gamma \approx 0.35$, which determines the shape of F_2 (see above), the corresponding stretching factors of the T_1 NMR spin-lattice relaxation measurements exhibit an increase resulting in less stretched magnetization transients. Obviously, spin-lattice relaxation NMR on the one hand and stimulated-echo NMR on the other hand are influenced by quite different correlation functions. Presumably, longitudinal relaxation is determined by a multiple-particle correlation function governed by (short-range) dipole-dipole interactions which are increasingly averaged with increasing T. In contrast to this, a single-spin correlation function is at the basis of quadrupolar stimulated-echo NMR, directly reflecting the nature of the hopping process without also being affected by multiple nuclear specific interactions.

V. SUMMARY AND CONCLUSION

In the present study we have investigated the application of ^{7}Li spin-alignment echo NMR to mixed conducting nanostructured materials of interest as promising electrodes in Li-ion batteries. Li self-diffusion parameters were extracted from preparation and mixing time-dependent echo decay functions. In the case of a mixed conductor this is, when conventional spin-lattice relaxation NMR techniques are applied in the temperature range covered here, usually fraught with difficulties such that insights into Li hopping processes are rarely available.

Interestingly, Li self-diffusion in nanowires of $Li_{0.3}TiO_2$-B seems to be highly heterogeneous. This manifests itself in correlation functions which can be fitted with stretched exponentials only. The decay rates determined by ^{7}Li SAE NMR indicate that overall Li hopping is rather slow. However, the material shows good performance when used as an anode in rechargeable Li batteries.[7–9] Obviously, the shorter e^- and Li^+ diffusion lengths in the nanowires compensate for this fact so that facile incorporation and removal of Li is possible while cycling a TiO_2-based battery.

ACKNOWLEDGMENTS

This work would not have been possible without the scientific and financial support of P. Heitjans (Leibniz University Hannover). We thank him for many fruitful and stimulating discussions as well as for allowing us to use his well equipped NMR laboratory in Hannover. The technical help of G. Schmidt (Bruker BioSpin GmbH, Germany) is highly appreciated.

*Author to whom correspondence should be addressed; wilkening@pci.uni-hannover.de
†pgb1@st-andrews.ac.uk

[1] M. Armand and J.-M. Tarascon, Nature (London) **451**, 652 (2008).
[2] J.-M. Tarascon, ChemSusChem **1**, 777 (2008).
[3] J.-M. Tarascon and M. Armand, Nature (London) **414**, 359 (2001).
[4] P. G. Bruce, B. Scrosati, and J.-M. Tarascon, Angew. Chem., Int. Ed. **47**, 2930 (2008).
[5] A. S. Aricò, P. Bruce, B. Scrosati, J.-M. Tarascon, and W. van Schalkwijk, Nature Mater. **4**, 366 (2005).
[6] M. S. Whittingham, Chem. Rev. (Washington, D.C.) **104**, 4271 (2004).
[7] A. R. Armstrong, G. Armstrong, J. Canales, and P. G. Bruce, Angew. Chem., Int. Ed. **43**, 2286 (2004).
[8] A. R. Armstrong, G. Armstrong, J. Canales, R. García, and P. G. Bruce, Adv. Mater. **17**, 862 (2005).
[9] A. R. Armstrong, G. Armstrong, J. Canales, and P. G. Bruce, Chem. Commun. (Cambridge) **2005**, 862.
[10] M. Wilkening, C. Mühle, M. Jansen, and P. Heitjans, J. Phys. Chem. B **111**, 8691 (2007).

[11] M. Wilkening, R. Amade, W. Iwaniak, and P. Heitjans, Phys. Chem. Chem. Phys. **9**, 1239 (2007).
[12] M. Wilkening, D. Gebauer, and P. Heitjans, J. Phys.: Condens. Matter **20**, 022201 (2008).
[13] S. Faske, H. Eckert, and M. Vogel, Phys. Rev. B **77**, 104301 (2008).
[14] M. Wilkening, W. Küchler, and P. Heitjans, Phys. Rev. Lett. **97**, 065901 (2006).
[15] M. Wilkening and P. Heitjans, Phys. Rev. B **77**, 024311 (2008).
[16] M. Wilkening, A. Kuhn, and P. Heitjans, Phys. Rev. B **78**, 054303 (2008).
[17] M. Wilkening, C. Lyness, A. R. Armstrong, and P. G. Bruce, J. Phys. Chem. C **113**, 4741 (2009).
[18] R. Böhmer, K. R. Jeffrey, and M. Vogel, Prog. Nucl. Magn. Reson. Spectrosc. **50**, 87 (2007).
[19] R. Böhmer, J. Magn. Reson. **147**, 78 (2000).
[20] F. Fujara, S. Wefing, and H. Spiess, J. Chem. Phys. **84**, 4579 (1986).
[21] G. Fleischer and F. Fujara, in *NMR—Basic Principles and Progress*, edited by P. Diehl, E. Fluck, H. Günther, R. Kosfeld, and J. Seelig (Springer, Berlin, 1994), Vol. 30.
[22] J. Jeener and P. Broekaert, Phys. Rev. **157**, 232 (1967).
[23] X.-P. Tang, R. Busch, W. L. Johnson, and Y. Wu, Phys. Rev. Lett. **81**, 5358 (1998).
[24] X.-P. Tang and Y. Wu, J. Magn. Reson. **133**, 155 (1998).
[25] X.-P. Tang, U. Geyer, R. Busch, W. Johnson, and Y. Wu, Nature (London) **402**, 160 (1999).
[26] R. Böhmer, T. Jörg, F. Qi, and A. Titze, Chem. Phys. Lett. **316**, 419 (2000).
[27] M. Wilkening and P. Heitjans, J. Phys.: Condens. Matter **18**, 9849 (2006).
[28] M. Wilkening and P. Heitjans, Solid State Ionics **177**, 3031 (2006).
[29] F. Qi, T. Jörg, and R. Böhmer, Solid State Nucl. Magn. Reson. **22**, 484 (2002).
[30] F. Qi, G. Diezemann, H. Böhm, J. Lambert, and R. Böhmer, J. Magn. Reson. **169**, 225 (2004).
[31] M. Wilkening and P. Heitjans, Defect Diffus. Forum **237-240**, 1182 (2005).
[32] F. Qi, C. Rier, R. Böhmer, W. Franke, and P. Heitjans, Phys. Rev. B **72**, 104301 (2005).
[33] R. Böhmer and F. Qi, Solid State Nucl. Magn. Reson. **31**, 28 (2007).
[34] E. Fukushima and S. Roeder, *Experimental Pulse NMR* (Addison-Wesley, Reading, 1981).
[35] R. Böhmer, S. Faske, and B. Geil, Solid State Nucl. Magn. Reson. **34**, 32 (2008).
[36] N. Bloembergen, E. M. Purcell, and R. V. Pound, Phys. Rev. **73**, 679 (1948).